

# Breaking the reflection law by asymmetric radiation pressure of intense circularly polarized light beam

Y. H. Tang,<sup>1</sup> Z. Gong,<sup>1</sup> J. Q. Yu,<sup>1</sup> Y. R. Shou,<sup>1</sup> and X. Q. Yan<sup>1,2,3,\*</sup>

<sup>1</sup>*State Key Laboratory of Nuclear Physics and Technology, Peking University, Beijing 100871, China*

<sup>2</sup>*CICEO, Shanxi University, Taiyuan, Shanxi 030006, China*

<sup>3</sup>*Shenzhen Research Institute of Peking University, Shenzhen 518055, China*

(Dated: April 20, 2022)

A novel deflection effect of an intense laser beam with spin angular momentum is revealed theoretically by an analytical modeling using radiation pressure and momentum balance in the relativistic regime of laser plasma interaction, as a deviation from the law of reflection. The reflected beam deflects out of the plane of incidence with an experimentally observable deflection angle, when an intense non-linear polarized laser is obliquely incident and reflected by an overdense plasma target. This effect originates from the asymmetric radiation pressure caused by spin angular momentum. A formula is given to predict the deflection angle of a Gaussian-type laser and reveal the relation between the angle and the parameters of laser and plasma, and is demonstrated by full three-dimensional particle-in-cell simulations of circularly polarized laser beams with different intensity and different pulse duration.

The earliest record about reflection of light can be retrospected in around 200 B.C., when Greek physicist Archimedes defended his homeland Syracuse, utilizing the giant mirror to set fire to invader's ships[1]. During the past two thousands years, humans have been persisting in pursuing the essential nature of reflection of light, which is summarized as the principle of interface conditions for electromagnetic fields in the classical optics[2]. The reflection of light at a plane interface is one of the most basic optical processes, which is ubiquitous in general optical system and experimental facilities[3–7]. The fundamental case, reflection of a plane wave at a perfectly flat interface between two homogeneous isotropic media, is characterized by the law of reflection and Fresnel equations[8]. The law of reflection claims that the direction of reflected light is in the plane of incidence, and the angle of reflection equals the angle of incidence. Nevertheless, the situation will become complicated when a realistic light beam possesses a finite spatial size and spectrum width, where the law of reflection is no longer valid. Neglecting shape deformations of the reflected beam, one can distinguish four basic deviations from the geometrical-optics picture. These deviations are usually referred as the spatial and angular Goos–Hänchen (GH)[9–14] and Imbert–Fedorov (IF)[15–17] shifts following commonly recognized terminologies[18].

The spatial GH shifts, originating from the dispersion of the reflection coefficients, displace the reflected beam within the plane of incidence[10]. In contrast, the effect of spatial IF shifts, pertinent to the conservation of angular momentum (AM) of light beam[19, 20], causes a displacement perpendicular to the plane of incidence to the reflected circularly polarized beam, which is also known as the spin Hall effect[21]. All above basic shifts can occur in a generic beam reflection and have a conse-

quent displacement at sub-wavelength scales. Apart from the spatial shifts, the angular shifts can be understood as shifts in the linear momentum space. The angular IF shift shows that the linear momentum of the reflected beam has a component perpendicular to the plane of incidence implying that the reflected beam deflects out of the plane of incidence, which is unveiled latterly[22–29].

However, these previous studies mainly focus on the weak light and the homogeneous isotropic media. In latest research, a new deflection of the reflected intense vortex laser beam similar to the angular IF shift was proposed in Ref[30], but the experimental infeasibility of the twisted wave front of such an intense short pulses deteriorates its significance. With the progress of state-of-the-art laser technologies, sub Peta-Watt laser facilities with an intensity of  $10^{20}$ W/cm<sup>2</sup> becomes available in practical experiments. When such a high-intensity pulse fires on the medium, it will ionize the materials into plasma within a temporal scale of femtoseconds, where the interaction between strong pulses and plasma is completely different from that of the weak light.

In this Letter, leveraging on theoretical analyses and fully self-consistent 3D PIC simulations, we present a novel phenomenon where the law of reflection is broken up when an intense non-linearly polarized laser is obliquely incident and reflected by an overdense plasma foil. This effect, issued from the deformation of the flat reflecting plane, is intrinsically induced by the antisymmetric radiation pressure of the circularly polarized laser pulse. Considering the balance between the radiation pressure and particles momentum, the dependence of the deflection angle  $\phi$  on the laser pulse intensity  $I_0$  and temporal duration  $\tau$  is analytically derived and improved by the numerical results of 3D simulations.

In order to investigate the radiation pressure exerted on foil surface by light beam, we turn to the interaction process between intense laser pulses and plasma, which is characterized by the synergy of Lorentz force and Maxwell equations. Neglecting the trivial colli-

\* x.yan@pku.edu.cn

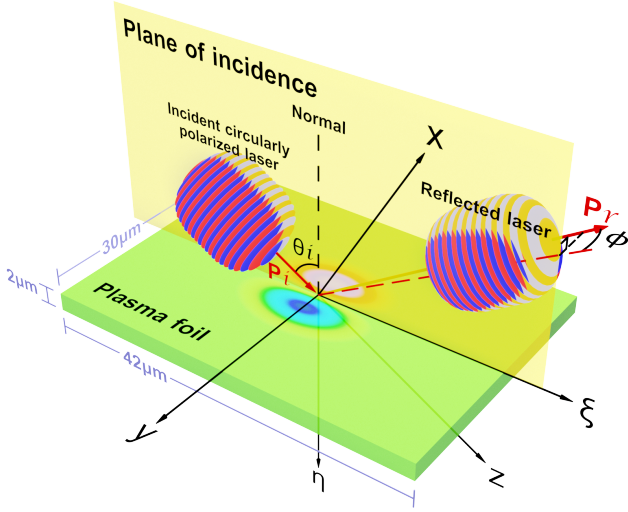


FIG. 1. Schematic diagram of reflection of an intense circularly polarized laser beam at a plane surface ( $\eta = 0$ ) of an overdense plasma foil. The coordinate frame  $(x, y, z)$  is attached to the incident beam, while the frame  $(\xi, y, \eta)$  is attached to the surface of the plasma foil. The laser beam, which propagate along  $z$ -axis and focus on the surface, is obliquely incident at an angle  $\theta$  and reflected by the plasma foil. The reflected beam deflects out of the plane of incidence ( $y = 0$ ) at a deflection angle  $\phi$ .

sions in plasma, the dominant force density is written as  $\mathbf{f} = \nabla \cdot \boldsymbol{\sigma} - (1/c^2)\partial\mathbf{S}/\partial t$ , where  $\mathbf{S} = (1/\mu_0)\mathbf{E} \times \mathbf{B}$  is the Poynting vector and  $\boldsymbol{\sigma}$  is the Maxwell stress tensor. The components of  $\boldsymbol{\sigma}$  read  $\sigma_{ij} = \varepsilon_0 (E_i E_j - \delta_{ij} E^2/2) + (1/\mu_0) (B_i B_j - \delta_{ij} B^2/2)$ , where  $\varepsilon_0$  the vacuum permittivity,  $\mu_0$  the vacuum permeability and  $\delta_{ij}$  Kronecker's delta. Integrating the force density  $\mathbf{f}$  over the interacting region, the total Lorentz force is expressed as  $\mathbf{F} = \oint_{\mathbf{a}} \boldsymbol{\sigma} \cdot d\mathbf{a} - (1/c^2)d(\int_V \mathbf{S} \cdot dV)/dt$ , where  $\mathbf{a}$  is the area of boundary surface and  $V$  is the closed volume, and Gauss's flux theorem is utilized when deriving the first term in  $\mathbf{F}$ . In practical interaction, as the laser pulse is totally reflected by the plasma target, only one side of foil's surface is irradiated by the electromagnetic pressure. The fields on other sides of surface and inside the foil are negligible, i.e.,  $\mathbf{S} \approx 0$  and  $\boldsymbol{\sigma}_{\text{inside}} \approx 0$ . Consequently, we get the radiation pressure caused by the electromagnetic field on the foil,  $\mathcal{P} = -d(\mathbf{F} \cdot \hat{\mathbf{n}})/ds = -(\boldsymbol{\sigma} \cdot \hat{\mathbf{n}}) \cdot \hat{\mathbf{n}}$ , where  $\hat{\mathbf{n}}$  is the unit normal vector of the foil surface. In the coordinate frame  $(x, y, z)$  of incident laser beam shown in Fig. 1,  $\hat{\mathbf{n}} = (\sin \theta_i, 0, -\cos \theta_i)$ , the pressure can be written as

$$\mathcal{P}_{las} = -(\sigma_{xx} \sin^2 \theta_i + \sigma_{zz} \cos^2 \theta_i - \sigma_{xz} \sin 2\theta_i). \quad (1)$$

The concrete form of  $\mathcal{P}_{las}$  can be determined if the Maxwell stress tensor  $\sigma_{ij}$  of laser beam is explicitly characterized. In the realm of intense laser plasma interaction, a beam with a Gaussian envelop is commonly recognized as the exact form of laser pulse. Under the paraxial

approximation, an eigen solution of the Maxwell equation in vacuum space prescribes the complex vector potential as  $\mathbf{A} = A_0(w_0/w) \exp[-(x^2 + y^2)/w^2] \exp\{i[\omega t - kz - k(x^2 + y^2)/2R + \psi(z)]\} (e_x \hat{\mathbf{x}} + e_y \hat{\mathbf{y}})$ , where  $A_0$  the amplitude constant,  $w_0$  the waist radius,  $w = w_0 \sqrt{1 + (z/z_R)^2}$  and  $R(z) = z[1 + (z_R/z)^2]$ .  $z_R = \pi w_0^2/\lambda$  the Rayleigh length and  $\lambda$  the laser wavelength.  $k = \omega/c$  the wave number,  $\hat{\mathbf{x}}$  and  $\hat{\mathbf{y}}$  unit vectors and  $\psi(z) = \arctan(z/z_R)$  the Gouy phase. The equation indicates that the wave propagates along the  $z$ -axis and the beam is focused at  $(0, 0, 0)$ . Leveraging on the Lorenz gauge condition, the electromagnetic fields can be derived from  $\mathbf{E} = -i\omega[\mathbf{A} + (c^2/\omega^2)\nabla\nabla \cdot \mathbf{A}]$  and  $\mathbf{B} = \nabla \times \mathbf{A}$ . After substituting the  $\mathbf{E}$  and  $\mathbf{B}$  into the formula of  $\boldsymbol{\sigma}$  and assuming  $\nabla\nabla \cdot \mathbf{A} \ll k^2 \mathbf{A}$ , we obtain the components of the effective Maxwell stress tensor

$$\begin{aligned} \langle \sigma_{xx} \rangle &= -\frac{1}{4} \varepsilon_0 A_0^2 \omega_0^2 \frac{x^2 + y^2}{z^2 + z_R^2} \exp\left(-2\frac{x^2 + y^2}{w_0^2}\right), \\ \langle \sigma_{zz} \rangle &= -\frac{1}{4} \varepsilon_0 A_0^2 \omega_0^2 \left(2 - \frac{x^2 + y^2}{z^2 + z_R^2}\right) \exp\left(-2\frac{x^2 + y^2}{w_0^2}\right), \\ \langle \sigma_{xz} \rangle &= -\frac{1}{2} \varepsilon_0 A_0^2 \omega_0^2 \frac{zx + sz_R y}{z^2 + z_R^2} \exp\left(-2\frac{x^2 + y^2}{w_0^2}\right). \end{aligned} \quad (2)$$

Here  $\langle \rangle$  denotes the temporal average over one laser period and  $s = 2\Im(e_x^* e_y)$  is the beam's helicity which represents its intrinsic spin angular momentum pertinent with the polarization states.  $s = 0$  corresponds to the linear polarization while  $s = 1$  ( $-1$ ) corresponds to the right (left) handed circular polarization. Substituting Eq. (2) into Eq. (1), we obtain the averaged radiation pressure of the incident beam

$$\langle \mathcal{P}_{las} \rangle = \frac{2I_0}{c} e^{-2(x^2 + y^2)/w_0^2} \left( \cos^2 \theta_i - s \frac{\lambda y}{\pi w_0^2} \sin 2\theta_i \right) \quad (3)$$

where non-grazing incident is assumed and high order terms are neglected. A factor of 2 is multiplied in Eq.(3) due to the effect of the reflected beam and  $I_0 = \varepsilon_0 c \omega^2 A_0^2/2$  is the peak intensity of the laser beam. The first term in Eq.(3) exhibits the isotropic properties which is symmetric along the transverse ( $y$ -axis) direction. However, the second term, induced by spin polarization, is proportional to the coordinate  $y$  which definitely results in an asymmetric distribution of radiation pressure with respect to the central axis  $y = 0$ .

To prove our theoretical analyses, self-consistent three dimensional particle-in-cell (PIC) simulations are performed via code EPOCH[31]. The simulation region is a box with size of  $50\mu\text{m} \times 40\mu\text{m} \times 40\mu\text{m}$ , which is uniformly divided into  $1000 \times 800 \times 800$  cells in  $x \times y \times z$  direction. A circularly polarized ( $s = 1$ ) Gaussian pulse with a temporal profile of  $e^{-(t-t_0)^4/\tau_0^4}$  is focused on the surface of foil, as shown in Fig. 1. The pulse possesses a wavelength  $\lambda = 1.0\mu\text{m}$ , a waist radius  $w_0 = 5.0\mu\text{m}$ , duration  $\tau_0 = 20\text{fs}$  and a peak intensity  $I_0 = 4.38 \times 10^{19}\text{W}/\text{cm}^2$ . The intensity corresponds to a normalized field amplitude

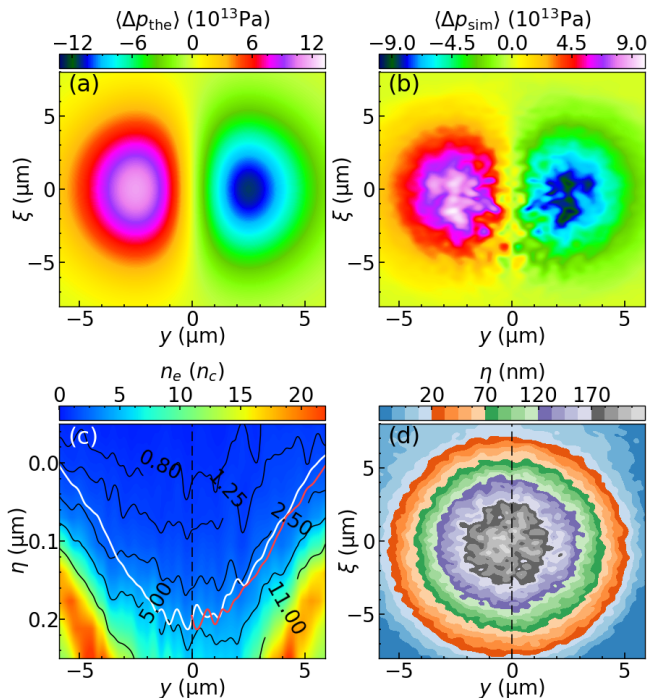


FIG. 2. (a) The theoretical periodic average pressure difference between  $(\eta, y, 0)$  and  $(\eta, -y, 0)$ . (b) The simulated periodic average pressure difference at  $t = 100$ fs when the laser is half reflected. (c) The electron density in simulation at  $\xi = 0$  and  $t = 150$ fs. The black lines are the isodensity lines, while the white line is the relativistic surface and the red line is its reflection with respect to  $y = 0$  for easy comparison. (d) The contour of the relativistic surface in simulation at  $t = 150$ fs when the reflection is finished.

$a_0 = eA_0/m_e c = 5.66$  (for circularly polarized pulse, the actual amplitude is  $a_0/\sqrt{2} = 4.0$ ). For simplicity, the incident angle is set as  $\theta_i = \pi/4$  and the pulse propagates along the  $z$ -axis, so that the reflected beam should propagate along the  $x$ -axis according to the law of reflection. The foil is a hydrogen plasma with an electron density of  $12n_c$  where  $n_c = \epsilon_0 m_e \omega^2 / e^2 = 1.1 \times 10^{21} \text{cm}^{-3}$  is the critical density[32]. The foil with a size of  $42 \mu\text{m} \times 30 \mu\text{m} \times 2 \mu\text{m}$  is put in  $\xi \times y \times \eta$  direction (as shown in Fig. 1) and the particles are represented by 16 macro-particles per cell for both electron and proton. The center of the irradiated surface is set coincidentally with the origin of the coordinate frame.

Induced by the antisymmetric radiation pressure with respect to the incident plane  $y = 0$  (the second term in Eq. (3)), the symmetry of the reflecting surface is deteriorated and the conventional reflecting law is no longer valid. The periodic averaged radiation pressure difference exerted on the reflecting surface  $\eta = 0$ ,  $\langle \Delta P(\xi, y) \rangle$ , is shown in Fig. 2, where the theoretical derived  $\langle \Delta P_{\text{the}} \rangle = -(2I_0 s \lambda y / \pi w_0^2 c) e^{-2(\xi^2 \cos^2 \theta_i + y^2)/w_0^2} \sin 2\theta_i$  is drawn in (a) while the pressure difference of 3D PIC simulation  $\langle \Delta P_{\text{sim}} \rangle$  is visualized in (b). The result in Fig. 2(b) cor-

responds temporally averaged value over one laser period at time  $t = 100$ fs, when the half of laser duration finishes being reflected by the surface.

When the high-intensity pulse irradiates on the plasma surface, the critical density for laser pulse being able to propagate through will be extended by the electrons' effective Lorentz factor  $\gamma_{\text{eff}}$ , which is also termed as relativistic induced transparency[33–36]. The asymmetric electron density distribution of reflecting surface, caused by the asymmetric pressure difference, is exhibited in Fig. 2(c) where the white line denotes the contour of relativistically correct critical density  $n_e = \gamma_{\text{eff}} n_c$  and  $\gamma_{\text{eff}} = \sqrt{1 + a^2} = \sqrt{1 + 16e^{-2(\xi^2 \cos^2 \theta_i + y^2)/w_0^2}}$ . The red line at  $y > 0$  is the axial symmetric part of white line at  $y < 0$  with respect to the incident plane  $y = 0$ , which demonstrates a pronounced depth difference in reflecting surface. The specific depth  $\eta$  of reflecting surface  $n_e = \gamma_{\text{eff}} n_c$  is plotted in Fig. 2(d), which indicates the left part is more deep than the right part as a result of the asymmetric radiation pressure.

To sustain such a reflecting cave, the laser pulse is inevitable to convert its energy (or momentum) into the plasma particles. The linear momentum of the electromagnetic field  $\mathbf{P} = \epsilon_0 \int_V (\mathbf{E} \times \mathbf{B}) dV$  is numerically integrated over the entire 3D simulation domain and the result is shown in Fig. 3(a), where  $P_z$  represents the momentum of the incident light while  $P_x$  implies that of the reflected beam. Starting from  $t \simeq 60$ fs,  $P_z$  quasi linearly drops down to zero until the  $t \simeq 140$ fs, indicating that the laser beam is totally reflected by the surface. The difference between final  $P_x$  and initial  $P_z$  implies that nearly 14% laser momentum is transferred into plasma particles. In Fig. 3(b), the transverse momentum  $P_y$  of the circularly polarized beam, exhibits the nonconservative feature during the reflection, which directly proves the projection of laser propagating direction is no longer zero in the transverse direction  $y$ -axis. To exclude the influence of IF effect, which is also able to result in a transverse deflection in surface reflection, we leverage on the AM of the electromagnetic wave  $\mathbf{L} = \epsilon_0 \int_V \mathbf{r} \times (\mathbf{E} \times \mathbf{B}) dV$ . The temporal evolution of AM is illustrated in Fig. 3(c). The AM is transferred to electrons and protons, so that the AM of electromagnetic field is no longer conserved which manifests intrinsic difference with respect to IF effect[28, 37].

Since the deformation of the reflecting surface evolves when being irradiated by the laser pulse, we can only get a mean deflection angle from  $\langle \phi \rangle = |P_y|/|\mathbf{P}| \simeq |P_y/P_x|$  where  $P$  represents the linear momentum of the reflected beam. The angle can be estimated as  $\langle \phi \rangle = 2.46 \text{mrad}$  when the reflection terminates and the momentum of the entire space represents that of the reflected beam at  $t = 150$ fs. The  $P_y$  of the p-linearly polarized beam with the same intensity is also shown in Fig. 3(b), and it's two orders of magnitude smaller than the circularly polarized beam. As shown in Fig. 3(c), the normal component of AM of field is no longer conserved in the condition, since the particles, triggered by the rotating laser electric

and magnetic field, continuously absorb energy from the helical topology of laser electric field in the azimuthal direction. It implies the broken of rotational symmetry with respect to the normal direction.

To determine which parameters impact on the deviating angle of the reflected light. The momentum balance of  $\eta$ -axis in the instantaneous rest frame, written as  $\langle p \rangle = 2n_i m_i v_\eta^2$ , is taken into account, where  $n_i$  is the ion density,  $m_i$  is the ion mass and  $v_\eta$  is the velocity of the plasma surface in the lab frame[38]. When the pulse is not a grazing incidence (i.e.  $|2\lambda sy \tan \theta / \pi w_0^2| \ll 1$ ), the velocity can be written as

$$v_\eta = \sqrt{\frac{I_0}{n_i m_i c}} e^{-(x^2+y^2)/w_0^2} \left( 1 - \frac{\lambda sy}{\pi w_0^2} \tan \theta \right). \quad (4)$$

We can find that for a non-linearly polarized beam, the plasma surface has different velocity with respect to the plane of incidence. The velocity of one side is larger than the other side, and it causes the surface tilted to one side. After the laser interaction with a duration  $\tau$ , there is a displacement difference  $\Delta\eta = \Delta v_\eta \tau$  between surface points  $(x_s, \pm y_s)$  where  $\Delta v_\eta$  is the velocity difference. The oblique angle of the plasma surface can therefore be expressed as  $\alpha = |\Delta\eta / 2y_s|$ . Using Eq. (4), we can obtain the oblique angle as

$$\alpha = \frac{\lambda \tau s \tan \theta}{\pi w_0^2} \sqrt{\frac{I_0}{n_i m_i c}} e^{-(x_s^2+y_s^2)/w_0^2}. \quad (5)$$

Via estimating the spatial averaged effect, the mean deflection angle of the reflected beam can be derived as

$$\langle \phi \rangle \simeq \alpha \sim \frac{\lambda \tau s \tan \theta}{\pi w_0^2} \sqrt{\frac{I_0}{n_i m_i c}}. \quad (6)$$

Based on the relation Eq. (6), the oblique angle of the reflective surface can be estimated as  $\alpha \simeq 2.1\text{mrad}$ , which corresponds well with the simulation result in Fig.2.

To further testify Eq. (6), a series of 3D PIC simulations with different laser intensity and pulse duration are performed. The numerical deflection angles in each simulations, calculated via  $\langle \phi \rangle = |P_y/P_x|$ , are shown in Fig. 3(d) as solid dots. The theoretical lines are obtained from Eq. (6) by replacing pulse duration  $\tau$  with the full width half maximum duration  $\tau_F = 2\sqrt[4]{\ln 2} \tau_0$  in simulation. As shown in Fig. 3(d), all lines are close to the simulation data points after multiplied by a same scale coefficient 0.62. It demonstrates the relation  $\langle \phi \rangle \propto \sqrt{I_0}$  and  $\langle \phi \rangle \propto \tau$ , which indicates that the effect is only pronounced for an intense laser and the deflection angle is increased with the raise of laser pulse duration.

In conclusion, a novel deflection effect of an intense laser with spin angular momentum is revealed by theoretical model and simulation, as a deviation from the law of reflection. The reflected beam deflects out of the

plane of incidence with an experimentally observable deflection angle, when an intense non-linear polarized laser

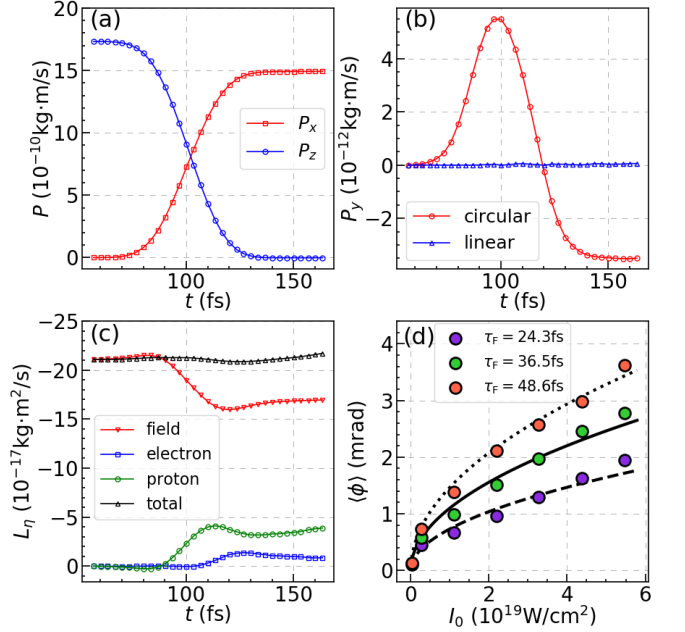


FIG. 3. (a)-(c) The temporal evolution of linear momentum  $\mathbf{P}$  and angular momentum  $\mathbf{L}$  for the entire space in simulation. (a)  $P_x$  (red squared line),  $P_z$  (blue circular line) of the field for the circular polarization. (b)  $P_y$  of the field for p-linear polarization (blue triangular line) and right circular polarization (red circular line). (c)  $L_\eta$  (the normal component of AM) of the field, particles and the total for the circular polarization. (d) Comparison of the deflection angles of the simulation results (the points) and the theoretical model (the lines) with different laser intensity and pulse duration.

is obliquely incident and reflected by an overdense plasma target. The analytical modeling is set up in the relativistic regime of laser plasma interaction, shows the asymmetric radiation pressure of a laser beam containing spin AM, and indicates the rotational symmetry breaking of the foil and the deflection of the reflected laser beam by momentum balance. A formula is given to predict the deflection angle of a Gaussian-type laser and reveal the relation between the angle and the parameters of laser and plasma. Finally, a succession of full three-dimensional PIC simulations of circularly polarized laser beams with different laser intensity and pulse duration demonstrate the relation between the angle and the laser intensity as well as the pulse duration.

## ACKNOWLEDGMENTS

The PIC code EPOCH was in part funded by the UK EPSRC grants EP/G054950/1, EP/G056803/1, EP/G055165/1 and EP/M022463/1. Simulations were supported by High-performance Computing Platform of Peking University.

- 
- [1] T. L. Heath *et al.*, *The works of Archimedes* (Courier Corporation, 2002).
- [2] J. D. Jackson, *Classical electrodynamics* (Wiley, 1999).
- [3] D. Strickland and G. Mourou, *Optics communications* **55**, 447 (1985).
- [4] C. Thaury, F. Quéré, J.-P. Geindre, A. Levy, T. Ceccotti, P. Monot, M. Bougeard, F. Réau, P. dOliveira, P. Audebert, *et al.*, *Nature Physics* **3**, 424 (2007).
- [5] D. Balabanski, R. Popescu, D. Stutman, K. Tanaka, O. Tesileanu, C. Ur, D. Ursescu, and N. Zamfir, *EPL (Europhysics Letters)* **117**, 28001 (2017).
- [6] O. Chekhlov, J. Collier, I. Ross, P. Bates, M. Notley, C. Hernandez-Gomez, W. Shaikh, C. Danson, D. Neely, P. Matousek, *et al.*, *Optics letters* **31**, 3665 (2006).
- [7] G. H. Miller, E. I. Moses, and C. R. Wuest, *Optical Engineering* **43**, 2841 (2004).
- [8] M. Born, E. Wolf, A. B. Bhatia, P. C. Clemmow, D. Gabor, A. R. Stokes, A. M. Taylor, P. A. Wayman, and W. L. Wilcock, *Principles of Optics: Electromagnetic Theory of Propagation, Interference and Diffraction of Light*, 7th ed. (Cambridge University Press, 1999).
- [9] F. Goos and H. Hänchen, *Annalen der Physik* **436**, 333 (1947).
- [10] K. Artmann, *Annalen der Physik* **437**, 87 (1948).
- [11] M. McGuirk and C. Carniglia, *JOSA* **67**, 103 (1977).
- [12] J. W. Ra, H. Bertoni, and L. Felsen, *SIAM Journal on Applied Mathematics* **24**, 396 (1973).
- [13] Y. M. Antar and W. M. Boerner, *Canadian Journal of Physics* **52**, 962 (1974).
- [14] C. C. Chan and T. Tamir, *Optics letters* **10**, 378 (1985).
- [15] F. Fedorov, *Dokl. Akad. Nauk SSSR* **105**, 465 (1955).
- [16] H. Schilling, *Annalen der Physik* **471**, 122 (1965).
- [17] C. Imbert, *Physical Review D* **5**, 787 (1972).
- [18] K. Y. Bliokh and A. Aiello, *Journal of Optics* **15**, 014001 (2013).
- [19] M. Player, *Journal of Physics A: Mathematical and General* **20**, 3667 (1987).
- [20] V. Fedoseyev, *Journal of Physics A: Mathematical and General* **21**, 2045 (1988).
- [21] M. Onoda, S. Murakami, and N. Nagaosa, *Physical review letters* **93**, 083901 (2004).
- [22] K. Y. Bliokh and Y. P. Bliokh, *Physical Review E* **75**, 066609 (2007).
- [23] K. Y. Bliokh, A. Niv, V. Kleiner, and E. Hasman, *Nature Photonics* **2**, 748 (2008).
- [24] O. Hosten and P. Kwiat, *Science* **319**, 787 (2008).
- [25] A. Aiello and J. Woerdman, *Optics letters* **33**, 1437 (2008).
- [26] A. Aiello, M. Merano, and J. Woerdman, *Physical Review A* **80**, 061801 (2009).
- [27] Y. Qin, Y. Li, X. Feng, Y.-F. Xiao, H. Yang, and Q. Gong, *Optics express* **19**, 9636 (2011).
- [28] K. Y. Bliokh, I. V. Shadrivov, and Y. S. Kivshar, *Optics letters* **34**, 389 (2009).
- [29] M. Merano, N. Hermosa, J. Woerdman, and A. Aiello, *Physical Review A* **82**, 023817 (2010).
- [30] L. Zhang, B. Shen, X. Zhang, S. Huang, Y. Shi, C. Liu, W. Wang, J. Xu, Z. Pei, and Z. Xu, *Physical review letters* **117**, 113904 (2016).
- [31] T. Arber, K. Bennett, C. Brady, A. Lawrence-Douglas, M. Ramsay, N. Sircombe, P. Gillies, R. Evans, H. Schmitz, A. Bell, *et al.*, *Plasma Physics and Controlled Fusion* **57**, 113001 (2015).
- [32] P. Gibbon, *Short Pulse Laser Interactions with Matter: An Introduction* (Imperial College Press, 2005).
- [33] P. Kaw and J. Dawson, *The Physics of Fluids* **13**, 472 (1970).
- [34] E. Lefebvre and G. Bonnaud, *Physical review letters* **74**, 2002 (1995).
- [35] B. Shen and Z. Xu, *Physical Review E* **64**, 056406 (2001).
- [36] L. Willingale, S. Nagel, A. Thomas, C. Bellei, R. Clarke, A. Dangor, R. Heathcote, M. Kaluza, C. Kamperidis, S. Kneip, *et al.*, *Physical review letters* **102**, 125002 (2009).
- [37] V. Fedoseyev, *Optics Communications* **282**, 1247 (2009).
- [38] A. Robinson, P. Gibbon, M. Zepf, S. Kar, R. Evans, and C. Bellei, *Plasma Physics and Controlled Fusion* **51**, 024004 (2009).